A Sephin1-insensitive tripartite holophosphatase dephosphorylates translation initiation factor 2α

Ana Crespillo-Casado[1*], Zander Claes[2], Meng S. Choy[3], Wolfgang Peti[3], Mathieu Bollen[2] and David Ron[1*]

From the [1]Cambridge Institute for Medical Research, University of Cambridge, Cambridge CB2 0XY, United Kingdom; [2]Department of Cellular and Molecular Medicine, KU Leuven, BE-3000 Leuven, Belgium; [3]Department of Chemistry and Biochemistry, University of Arizona, Tucson, Arizona 85721-0041, United States

Running title: *Reconstitution of a PPP1R15A-containing holophosphatase*

*To whom correspondence should be addressed: Ana Crespillo-Casado & David Ron: Cambridge Institute for Medical Research, University of Cambridge, Cambridge Biomedical Campus, Wellcome Trust/MRC Building, Hills Road, Cambridge CB2 0XY, United Kingdom; ac880@cam.ac.uk & dr360@medschl.cam.ac.uk; Phone +44 (0)1223 768 940

ABSTRACT

The integrated stress response (ISR) is regulated by kinases that phosphorylate the α subunit of translation initiation factor 2 and phosphatases that dephosphorylate it. Genetic and biochemical observations indicate that the eIF2α^P-directed holophosphatase - a therapeutic target in diseases of protein misfolding - is comprised of a regulatory, PPP1R15, and a catalytic, Protein Phosphatase 1 (PP1) subunit. In mammals, there are two isoforms of the regulatory subunit, PPP1R15A and PPP1R15B, with overlapping roles in the essential function of eIF2α^P dephosphorylation. However, conflicting reports have appeared regarding the requirement for an additional co-factor, G-actin, in enabling substrate-specific dephosphorylation by PPP1R15-containing PP1 holoenzymes. An additional concern relates to the sensitivity of the holoenzyme to the [(o-chlorobenzylidene)amino]guanidines Sephin1 or Guanabenz, putative small molecule proteostasis modulators. It has been suggested that the source and method of purification of the PP1 catalytic subunit and the presence or absence of an N-terminal repeat-containing region in the PPP1R15A regulatory subunit might influence the requirement for G-actin and sensitivity of the holoenzyme to inhibitors. We find that eIF2α^P-dephosphorylation by PP1 was moderately stimulated by repeat-containing PPP1R15A in an unphysiological low ionic strength buffer, whereas stimulation imparted by the co-presence of PPP1R15A and G-actin was observed under a broad range of conditions: low and physiological ionic strength; whether PPP1R15A regulatory subunit had or lacked the N-terminal repeat-containing region; and whether it was paired with native PP1 purified from rabbit muscle, or recombinant PP1 purified from bacteria. Furthermore, none of the PPP1R15A-containing holophosphatases tested was inhibited by Sephin1 or Guanabenz.

The integrated stress response (ISR) is a signal transduction pathway that couples diverse stressful conditions to the activation of a rectifying translational and transcriptional program that is implicated in biological processes ranging from memory formation to immunity and metabolism (reviewed in Ref. 1). The mammalian ISR and its yeast counterpart (the general control response) are initiated by the phosphorylation of the α subunit of translation initiation factor 2 (eIF2α) on

serine 51 (2,3) and its activity is terminated by eIF2α[P] dephosphorylation.

Two related regulatory proteins, PPP1R15A/GADD34 and PPP1R15B/CReP, encoded in mammals by *PPP1R15A* and *PPP1R15B*, direct the unspecific Protein Phosphatase 1 (PP1) to promote eIF2α[P] dephosphorylation (4-7). PPP1R15A or PPP1R15B form a complex with PP1 via a conserved region of ~70 amino acids (PPP1R15A residues 555-624) located at their C-termini (5,8-11) ([Fig. 1*A*]). This conserved C-terminal region of either PPP1R15 regulatory subunit is sufficient to promote eIF2α[P] dephosphorylation and to inactivate the ISR (4,5,10,11). Indeed, Herpes viruses have exploited this activity and encode a small protein homologous to the C-terminus of PPP1R15 to reverse eIF2α phosphorylation, undoing a defensive strategy of infected cells (12).

Despite genetic evidence pointing to the sufficiency of the conserved C-terminal portion of PPP1R15 in reversing the eIF2α[P]-dependent ISR *in vivo* (4,5,10), complexes formed *in vitro* between PPP1R15 regulatory subunit fragments and PP1 have not been observed to accelerate eIF2α[P] dephosphorylation: dephosphorylation of eIF2α[P] is no faster by a complex of PPP1R15A-PP1 (or PPP1R15B-PP1) than by PP1 alone, showing that when added as single components, PPP1R15A/B do not influence k_{cat} or K_m of PP1 towards the substrate eIF2α[P] (10). However, addition of G-actin to the binary complex of PPP1R15 and PP1 selectively accelerates eIF2α[P] dephosphorylation. G-actin binds directly to the conserved C-terminus of PPP1R15, alongside PP1 to form a ternary complex, whose affinity ($K_d \sim 10^{-8}$ M) matches the EC_{50} of G-actin's stimulatory effect (10,13). The *in vivo* relevance of G-actin to eIF2α[P] dephosphorylation is attested to by the finding that actin sequestration in fibres (as F-actin) enfeebles eIF2α[P] dephosphorylation, implying a role for factors that affect the actin cytoskeleton in ISR regulation (14).

The ability to dephosphorylate eIF2α[P] is an essential function in developing mammals (15). Nonetheless, inactivation of the *PPP1R15A* gene, which decelerates eIF2α[P] dephosphorylation and prolongs the ISR, is protective in certain cellular and animal models of diseases associated with enhanced unfolded protein stress (16-19). This has generated interest in targeting the PPP1R15A-

containing holophosphatase for inhibition by small molecules (reviewed in Ref. 20); an endeavour that requires detailed knowledge of the enzymatic mode of action.

A recent report challenged the need for G-actin as a co-factor in PPP1R15A-mediated eIF2α[P] dephosphorylation (21). Instead, it suggested that a binary complex assembled from PP1α and a fragment of PPP1R15A (PPP1R15A[325-636]), encompassing both the C-terminal PP1-binding region and the N-terminal repeat-containing extension, dephosphorylates eIF2α[P] faster than PP1 alone (21). Importantly, dephosphorylation of eIF2α[P] by this active binary complex was reported to be selectively inhibited *in vitro* by Guanabenz and Sephin1, two structurally-related small molecules that function *in vivo* as proteostasis modifiers (22,23). The new study contradicts previous observations that neither a PPP1R15A-PP1 binary complex, nor a PPP1R15A-PP1-G-actin ternary complex, were susceptible to inhibition by Guanabenz or Sephin1 (9,13).

Here we address three important questions raised by these discrepant reports: Does the isotype of PP1 catalytic subunit or its source (recombinant versus native) influence the requirement for G-actin by the eIF2α[P]–directed holophosphatase? What role does the N-terminal repeat-containing region of PPP1R15A play in eIF2α[P] dephosphorylation by the holophosphatase? Do these factors influence the sensitivity of eIF2α[P] dephosphorylation to Guanabenz and Sephin1?

Results

Both native PP1 and bacterially-expressed PP1α require the presence of G-actin to promote PPP1R15A-regulated eIF2α[P] dephosphorylation

PP1 produced in *E. coli* may differ in its enzymatic activity from PP1 purified from animal tissues, both in its substrate specificity and in its sensitivity to regulatory subunits (reviewed in ref. 24). To determine if the G-actin-dependence of PP1-PPP1R15A-mediated eIF2α[P] dephosphorylation is a peculiarity of the bacterially-expressed PP1γ isoform used previously (10,13), we purified the native catalytic subunit of PP1 from rabbit skeletal muscle (PP1[N]), following an established protocol (25), and compared the two PP1 preparations. Native PP1

($PP1^N$) is a mixture of PP1α, PP1β and PP1γ isoforms and gave rise to two prominent bands on SDS-PAGE (**Fig. S1*A***, left panel). The mass spectra of tryptic peptides derived from the $PP1^N$ sample was analysed by Maxquant with iBAQ (intensity based absolute quant) to identify the major contaminating species (tropomyosin), and to estimate the relative contribution of PP1 and contaminants to the protein preparation. This enabled a comparison of the catalytic subunit content of $PP1^N$ preparation with the bacterially-expressed PP1γ, which served as a reference.

The N-terminal portion of PPP1R15A, which includes the membrane association region (26), compromises expression in bacteria and recovery of a functional protein (27). Therefore, we used a $PPP1R15A^{325-636}$ fragment lacking this region, which is soluble when expressed in *E. coli*. **Fig. 1*B*** shows that addition of either $PPP1R15A^{325-636}$-MBP (lanes 5-8), or G-actin alone (lanes 13 & 14) did not stimulate $eIF2α^P$ dephosphorylation by nanomolar concentrations of $PP1^N$. However, addition of both G-actin and $PPP1R15A^{325-636}$-MBP (lanes 9-12) stimulated dephosphorylation by 5-fold (**Fig. 1*B***), similar to the increase observed with bacterially expressed PP1γ (**Fig. S1*B***)(10).

PP1 purified from rabbit muscle is a mixture of α, β and γ isoforms, whereas it has been reported that the PP1α isoform possesses *in vivo* selectivity for PPP1R15A (6). Therefore, we prepared bacterially-expressed PP1α by a method that promotes its native-like state (28). To control for effects the location of the tag might have on activity, we also generated an N-terminally MBP-tagged $PPP1R15A^{325-636}$ (MBP-$PPP1R15A^{325-636}$, **Fig. 1*A*, Table S1**). The holophosphatase comprised of PP1α and MBP-$PPP1R15A^{325-636}$ also exhibited a stringent requirement for G-actin (**Fig. 1*C***).

A concentration-dependent stimulatory effect of PPP1R15A on $eIF2α^P$ dephosphorylation by the three component holoenzyme (PP1, PP1R15A and G-actin) was observed with constructs tagged at either their N- or C-termini and with either native or bacterially-expressed PP1 (**Fig. 2*A* and *B***). The difference in EC_{50} values obtained for $PPP1R15A^{325-636}$-MPB with $PP1^N$ (58 nM) or MBP-$PPP1R15A^{325-636}$ with PP1α (6 nM) may reflect the effect of the position of the MBP-tag, the contaminating tropomyosin (in $PP1^N$), or

both. Importantly, the data agreed with similar experiments in which $PPP1R15A^{325-636}$ and bacterially-expressed PP1γ were used, EC_{50} of 10 nM (13, Figure 8A therein).

G-actin also exerted a saturable concentration-dependent stimulatory effect on the activity of a three-component holophosphatase constituted with native $PP1^N$ (**Fig. 2*C***). The EC_{50} for G-actin with $PP1^N$ (30 nM) was similar to that previously observed using bacterially-expressed PP1γ, EC_{50} of 13 nM (13, figure 2C therein). Hence, despite variations in the estimated EC_{50} values for PPP1R15A or G-actin, the combinations of catalytic and regulatory subunits tested showed consistent PPP1R15A and G-actin concentration dependent enzymatic activity. These experiments, conducted in a buffer of physiological ionic strength, over a physiological protein concentration range (nanomolar catalytic subunit and micromolar substrate) and over a timescale aimed to minimize the effect of substrate depletion on enzyme kinetics, indicate that neither the source of PP1 nor the position of the tag in PPP1R15A are likely to account for the reported G-actin independent ability of PPP1R15A to stimulate $eIF2α^P$ dephosphorylation.

Two-fold stimulation of $eIF2α^P$ dephosphorylation by repeat-containing PPP1R15A in an unphysiological low ionic strength buffer

To explore the discrepant findings on the G-actin independent stimulatory activity of MBP-$PPP1R15A^{325-636}$ we sought to reproduce the experiments reported in reference 21 as closely as possible. We received from the Bertolotti laboratory their expression plasmid. The encoded protein, referred to here as MBP~$PPP1R15A^{325-636}$ (**Fig. 1*A***) differs from the one used above (MBP-$PPP1R15A^{325-636}$) by the absence of three residues in the linker separating the MBP from PPP1R15A and 11 residues in the linker separating PPP1R15A from the C-terminal poly-histidine tag (see **Table S1**). The MBP~$PPP1R15A^{325-636}$ fusion protein was produced in *E. coli* and purified as described (21) and dephosphorylation reactions were carried out in a salt-free, low ionic strength buffer, designed to mimic as close as possible the one used in that study (50 mM Tris at pH 7.4, 1.5 mM EGTA, 2 mM $MnCl_2$, with the notable

3

exception of 0.5 mM TCEP, added here to prevent inactivation of the catalytic subunit by oxidation).

A 2-fold stimulation of eIF2α^P dephosphorylation by MBP~PPP1R15A$^{325\text{-}636}$ was apparent in reactions conducted at low salt concentration (15 mM), but lost at more physiological concentrations (100 mM), whilst the 5-fold stimulatory effect of G-actin was observed at both low and physiological salt concentration (**Fig. 3*A***). The stimulatory effect of MBP~PPP1R15A$^{325\text{-}636}$ at low salt concentration was dependent on the N-terminal repeat-containing region of PPP1R15A (**Fig 3*B***), as reported (21), and was not observed with a non-specific dephosphorylation substrate (**Fig. S2*A***).

Though modest (two-fold) and confined to non-physiological, low ionic strength conditions, this stimulatory effect was reproducibly observed also with the MBP-PPP1R15A$^{325\text{-}636}$ and PPP1R15A$^{325\text{-}636}$-MBP proteins used in Fig.1 and Fig.2 (**Fig. S2*B***), negating a role for the linkers or the position of the tag in this activity. Notably, in both unphysiological-low ionic strength buffer (in which PPP1R15A alone has a stimulatory effect) and in physiological conditions, the presence of G-actin dominates the kinetics of eIF2α^P dephosphorylation.

Lengthy incubation of the enzymatic reactions does not uncover PPP1R15A's ability to promote G-actin-independent eIF2α^P dephosphorylation at physiological salt concentrations

Upon inhibition of the phosphorylating kinase, the eIF2α^P signal decays with a $T_{1/2}$ of <10 minutes (with no change in the total eIF2α content) in both cultured mouse fibroblasts (Ref. 14, figure 6 therein) and Chinese Hamster Ovary cells (Ref. 13, figure 10 therein). Despite the rapid *in vivo* kinetics of the dephosphorylation reaction, the experiments pointing to G-actin-independent eIF2α^P dephosphorylation were conducted with long incubations of 16 hours at 30˚C (21). In the absence of other components, PP1α is markedly unstable at 30˚C, losing about half of its activity by 1 hour and all detectable activity by 3 hours (**Fig. S3*A* and *B***). Thus, a stabilizing effect of a PP1 binding co-factor might have accounted for the apparent G-actin-independent stimulatory effect of MBP-PPP1R15A$^{325\text{-}636}$ on PP1α-mediated eIF2α^P dephosphorylation at physiological salt concentrations. However, over a range of PP1 concentrations (0.2-200 nM), the presence of MBP-PPP1R15A$^{325\text{-}636}$ failed to stimulate eIF2α^P dephosphorylation, whether PP1^N (**Fig. 4*A***) or PP1α (**Fig. 4*B***) were used as the catalytic subunit.

Substrate recruitment by the repeat-containing PPP1R15A$^{325\text{-}512}$ region plays a secondary role in the kinetics of eIF2α^P dephosphorylation and its disruption is unlikely to account for sensitivity to Sephin1

PPP1R15A interacts directly with eIF2α, both in cells (9) and *in vitro* (21). This interaction maps to the repeat-containing region of PPP1R15A, residues 325-512; N-terminal to PPP1R15A's PP1-binding domain (**Fig. 1*A***) and was proposed to play an important role in the catalytic cycle of PPP1R15A-containing holoenzymes (21). However, in the presence of G-actin, PPP1R15A$^{325\text{-}636}$-MBP and PPP1R15A$^{533\text{-}624}$-MBP (**Fig. 1*A*, Table S1**) stimulated eIF2α^P dephosphorylation similarly, when paired either with PP1^N (compare **Fig. 2*B*** and **5*A*** here) or with PP1γ (compare Figure 8A and Figure 2B in Ref. 13). These findings suggest that the conserved C-terminal PPP1R15 fragment that binds PP1 and G-actin simultaneously is sufficient to promote eIF2α^P dephosphorylation and to dominate its kinetics *in vitro* and call in to question the importance of the N-terminal repeats in PPP1R15A to the fundamentals of the holoenzyme's catalytic cycle.

We considered that an important contributory role for substrate engagement by the PPP1R15A$^{325\text{-}533}$ repeat-containing fragment to the catalytic cycle of the holophosphatase might have been masked by compensatory features that diverge between the different regulatory subunit constructs, fortuitously equalizing their activity. To address this possibility, we measured the ability of MBP-PPP1R15A$^{325\text{-}512}$ containing the repeats but lacking the C-terminal PP1 binding region (**Fig. 1*A***, **Table S1**) to compete with MBP-PPP1R15A$^{325\text{-}636}$-mediated (G-actin-dependent) eIF2α^P dephosphorylation using PP1α as the catalytic subunit. Minimal inhibition of the dephosphorylation reaction was observed at competitor concentrations of up to 8 µM (**Fig. 5*B***), which is a >300-fold excess over the MBP-PPP1R15A$^{325\text{-}636}$ regulatory subunit (present in the reaction at 24 nM), and a concentration of 18-fold

above the reported K_d of the interaction between MBP-PPP1R15A$^{325-512}$ and eIF2α^P (21).

These data suggest that substrate recruitment by the N-terminal extension of PPP1R15A plays a secondary role in the kinetics of the dephosphorylation reaction *in vitro* and that the reported role of Sephin1 and Guanabenz in disrupting that interaction is unlikely to make an important contribution to their pharmacological activity. Consistent with these conclusions we find that under physiological salt conditions in which eIF2α^P dephosphorylation is dependent on the concentration of PP1α, MBP-PPP1R15A$^{325-636}$ and G-actin, we were unable to observe an inhibitory effect of either Sephin1 (**Fig. 6*A*** and **Fig. S4*A***, lanes 8-11) or Guanabenz (**Fig. 6*B*** and **Fig. S4*B***, lanes 7-10) at a concentration of up to 100 µM which exceeds by a hundred-fold the concentration required for a proteostatic effect in cultured cells (1 µM)(23, figure 1F therein). Similarly, no effect of the compounds was observed on the PP1-PPP1R15A holophosphatase activity in low salt conditions (**Fig. S4*A*** lanes 1-7 and **Fig. S4*B*** lanes 1-6).

Complete inhibition of PPP1R15A-mediated eIF2α^P –dephosphorylation by Sephin 1 was reported in an assay conducted over 16 hours at 30˚C in a low ionic strength buffer (21). We wished to test if the reported Sephin1's inhibition might be unmasked by this long incubation (in which the enzyme is undergoing inactivation, **Fig. S3*B***). Using identical MBP~PPP1R15A$^{325-636}$ and PP1α constructs, in an identical low ionic strength buffer and following overnight incubation at 30˚C, we observed a two-fold stimulation of eIF2α^P–dephosphorylation by MBP~PPP1R15A$^{325-636}$ (similar to that noted in shorter reactions **Fig. 3)**. However, even in these conditions, designed to mimic as closely as possible those used in reference (21), the presence of 100 µM Sephin1 was devoid of an inhibitory effect on substrate dephosphorylation (**Fig. S4*C***)

Discussion

The new experiments presented here cover a range of conditions with realistic concentrations and time regimes. Incorporation of multiple time points and titrations of reaction components enabled a comparison of enzyme kinetics that accounts for the effect of substrate depletion. Our observations were made with four different PPP1R15A preparations, three different PP1 preparations and both buffer conditions previously used in our lab and those used in reference (21), all of which consistently show the requirement for G-actin as an additional co-factor in enabling PPP1R15A to stimulate eIF2α^P dephosphorylation *in vitro*. As such the results presented here are in keeping with previous observations that G-actin has an essential role in promoting eIF2α^P dephosphorylation both *in vitro* and *in vivo* (10,13,14).

The PP1 apo-enzyme is salt sensitive and inhibited by buffers of physiological ionic strength (29). By contrast, PP1-holoenzymes retain their regulated enzymatic activity at physiological ionic strength (30). These considerations call into question the significance of the two-fold stimulation of eIF2α^P dephosphorylation by PPP1R15A$^{325-636}$ observed in buffer of low ionic strength. Our experiments also cast doubt on the importance of the physical interaction between the repeat-containing region of PPP1R15A (residues 325-512) and eIF2α^P in substrate-specific dephosphorylation reaction carried out in physiological ionic strength. PPP1R15 regulatory subunits are found throughout the animal kingdom, yet only their C-terminal ~70 residues are conserved (11). This C-terminal fragment contains all the information needed to promote eIF2α^P dephosphorylation, as exemplified by its selective hijacking by Herpes viruses (12) and by experimentally targeted expression in cells (10, figure 1C therein). In complex with G-actin, the conserved C-terminal fragment of the PPP1R15s is also able to direct PP1 to selectively dephosphorylate eIF2α^P *in vitro* (**Fig. 2 and 5*A*** here and (10,13).

The prominent stimulatory role of G-actin on eIF2α^P dephosphorylation, observed both *in vivo* and *in vitro*, should not obscure the possibility that binary complex formation with PPP1R15 might also favour eIF2α^P dephosphorylation independently of G-actin joining the complex. Regulatory subunit binding restricts access to PP1 (24,31), favouring the phosphorylation of one class of substrates over another. Mere exclusion of some substrates from access to the catalytic subunit might accelerate eIF2α^P dephosphorylation when levels of PPP1R15A levels are sufficiently elevated in cells – even though *in vitro* (and in the absence of

competing substrates) the PPP1R15A-PP1 binary complex is not a faster eIF2α^P phosphatase than PP1 alone (provided the experiments are conducted at physiological salt concentrations). As neither Sephin1 nor Guanabenz affect the stability of the PPP1R15A-PP1 complex (13), it is unlikely that they achieve any measure of inhibition by weakening PPP1R15A's ability to compete with other regulatory subunits for limiting amounts of catalytic subunit. These considerations lead us to propose a dual role for PPP1R15A in cells: Diverting limiting amounts of PP1 away from other substrates towards eIF2α^P and, in conjunction with G-actin as an essential co-activator, stimulating the intrinsic rate of dephosphorylation by the holoenzyme thus formed. Actin, too, has a dual role in stimulating eIF2α^P dephosphorylation: by stabilizing the PPP1R15-PP1 complex (14) G-actin favours the exclusion of other regulatory subunits, whilst stimulating enzyme kinetics selectively towards eIF2α^P (**Fig. 7**).

Here we present no argument against an important function for the divergent N-terminal extensions of PPP1R15 regulatory subunits. This role may play out in terms of subcellular localization (26) or protein stability (32) and might be influenced by a physical interaction with the substrate (9,21). However, our findings argue that the physical interaction noted previously between PPP1R15A residues 325-512 and eIF2α^P (21) is unlikely to play an important role in formation of the enzyme-substrate complex required for catalysis under physiological conditions and hence its disruption by Guanabenz or Sephin1 is unlikely to underscore an inhibitory effect on eIF2α^P dephosphorylation.

Most importantly perhaps, the findings presented here argue that the inability of previous efforts to uncover a role for Guanabenz or Sephin1 in inhibiting eIF2α^P dephosphorylation *in vitro* (9,13) was unlikely to have arisen from choice of catalytic subunit, from features of the PPP1R15A regulatory subunit or the buffer conditions used. Rather, the findings reported here, made *in vitro*, reinforce observations that Sephin1 and Guanabenz have no measurable effect on the rate of eIF2α^P dephosphorylation in cells (13). The recent description of PPP1R15A/GADD34-independent cellular effects of Guanabenz (33) and our observations that Sephin1-induced

changes in gene expression were noted both in cells lacking PPP1R15A and in cells with non-phosphorylatable eIF2α (13), suggest the need to reconsider the role of these two compounds as eIF2α^P dephosphorylation inhibitors.

Experimental procedures
Protein expression and purification

The plasmids used to express protein in *E. coli* and the sequence of the encoded proteins are listed in **Tables S1** and **S2**.

PPP1R15A$^{325-636}$-MBP and PPP1R15A$^{533-624}$-MBP were produced as described (13). Briefly, proteins were expressed in *E. Coli* BL21 (New England Biolabs, Cat. No.C3013) as N-terminally-tagged glutathione S-transferase fusion proteins and were purified by tandem affinity chromatography, first bound to a glutathione sepharose 4B resin, eluted with glutathione, followed by an overnight cleavage with Tobacco Etch Virus (TEV) protease (to remove the GST tag), binding to amylose beads and elution in maltose-containing buffer.

MBP-PPP1R15A$^{325-636}$ and MBP-PPP1R15A$^{325-512}$ were constructed in the C-terminally hexahistidine tag-containing pMAL-c5x-His plasmid (New England Biolabs, Cat. No. N8114). Transformed *E. Coli* BL21 (New England Biolabs, Cat. No. C3013) were selected on LB agar plates supplemented with 100 μg/ml ampicillin. A single colony was picked to grow overnight in 5 mL starter culture that served to inoculate 2 L of LB media (all supplemented with 100 μg/mL ampicillin), which was kept at 37°C. At OD$_{600}$=0.6-0.8 protein expression was induced using 1 mM Isopropyl β-D-1-thiogalactopyranoside (IPTG) at 18°C for 20 hours. Bacteria were pelleted and resuspended in ice-cold His6 Lysis Buffer containing 50 mM Tris pH 7.4, 500 mM NaCl, 1 mM MgCl$_2$, 1 mM tris (2-carboxyethyl)phosphine (TCEP), 100 μM phenylmethylsulfonyl fluoride (PMSF), 20 mTIU/ml aprotinin, 2 μM leupeptin, and 2 μg/ml pepstatin 20 mM imidazole and 10% glycerol. Bacterial suspensions were lysed using an Emulsi-Flex-C3 homogenizer (Avestin, Inc, Ottawa, Ontario) and clarified in a JA-25.50 rotor (Beckman Coulter) at 33,000 x g for 30 min at 4°C. Pre-equilibrated Ni-NTA beads (Qiagen, Cat. No. 30230,) were incubated with the samples for 2

hours at 4°C. Proteins were eluted in 2 mL of imidazole elution buffer (50 mM Tris, pH 8, 100 mM NaCl, 500 mM imidazole, 10% glycerol) and incubated with amylose beads (New England Biolabs, Cat No. E8021S) pre-equilibrated with lysis buffer (His6 lysis buffer without imidazole) for 2 hours at 4°C. The amylose beads were batch-washed using 25 bed volumes of lysis buffer and proteins were eluted with amylose elution buffer (lysis buffer + 10 mM maltose). MBP-R15A[325-512] purification required an additional buffer exchange step (into lysis buffer) using Centripure P1 de-salting columns (EMP Biotech, Cat. No. CP-0110) to eliminate maltose (that appeared to interfere with the dephosphorylation reactions when present at high concentrations).

MBP~PPP1R15A[325-636] (a gift of the Bertolotti lab) was expressed and purified as described (21), with minor modifications: The IPTG-induced culture was maintained for 16 hours at 18°C and 0.5 mM TCEP was included in all buffers, throughout the purification procedure and in the final dialysis buffer (50 mM Tris at pH 7.4, 200 mM NaCl, 0.5 mM TCEP).

eIF2α[P]**:** The N-terminal fragment of human eIF2α (1-185, with three solubilizing mutations) was purified from bacteria and phosphorylated *in vitro* using the kinase domain of PERK, as described (10).

G-actin was purified from rabbit muscle according to ref. (34) as modified in ref. (10).

PP1γ (7-300) was purified according to ref. (13).

PP1α (7-330) was purified from BL21 *E. coli* according to ref. (28,35)

PP1[N] was purified from rabbit muscle according to ref. (25)

In vitro dephosphorylation reactions

Unless otherwise stated, dephosphorylation reactions were performed at a final volume of 20 µL by assembling 5 µL of 4× solution of each component: PP1, PPP1R15A, G-actin and eIF2α[P] (or their respective buffers). A 10X assay buffer (500 mM Tris pH 7.4, 1 M NaCl, 1 mM EDTA, 0.1% Triton X-100, 10 mM MgCl$_2$) was diluted 1:10, supplemented with 1 mM DTT and used to create working solutions of PP1, PPP1R15A and eIF2α[P] at the desired concentrations. G-actin working solutions were created using G-buffer (2 mM Tris-HCl at pH 8, 0.2 mM ATP, 0.5 mM DTT and 0.1 mM CaCl$_2$).

Holoenzyme components (PP1, PPP1R15A and G-actin) were combined first and substrate (eIF2α[P]) was added last to initiate the reactions, which were conducted under shaking at 500 rpm and at 30°C for the specified time. The final buffer composition was 36 mM Tris pH 7.4, 76 mM NaCl, 74 µM EDTA, 0.007 % Triton X-100, 0.7 mM MgCl$_2$, 25 µM CaCl$_2$, 0.05 mM ATP and 0.8 mM DTT, 0.5 µM Latrunculin B, 0.4 - 3 µM MnCl$_2$, 0.5% Glycerol and 50 µM TCEP, in experiments performed in **Fig. 1**, **Fig. 2**, **Fig. 4**, **Fig. 5**, **Fig. 6**, **Fig. S1**, **Fig. S3** and **Fig. S4***A* (lanes 8-11) and **Fig. S4***B* (lanes 7-10).

Dephosphorylation reactions designed to reproduce the observations of ref. (21) were performed in the assay buffer described therein (50 mM Tris-HCl pH 7.4, 1.5 mM EGTA pH 8.0, 2 mM MnCl$_2$), with the modification that 0.5 mM TCEP was added to disfavor oxidative inactivation of the enzyme. The NaCl content of the final reaction was constrained by the contribution of the protein solutions added to each reaction. To maintain parity between reactions performed with and without PPP1R15A, an equal volume of the PPP1R15A buffer was added to reactions lacking the protein. The final salt concentration in the various reactions is noted in the figure legends.

The stability test of PP1α (**Fig. S***3*) was performed by preparing a fresh 240 nM solution of PP1α in the assay buffer described above. Separate aliquots were pre-incubated either at 30°C or on ice for the specified times (30 minutes to 7 hours, see schema in **Fig. S3***A*). At termination of the pre-incubation, 5 µL of these pre-incubated solutions were added into 20 µL dephosphorylation reactions as described above.

Dephosphorylation reactions to test the activity of Sephin1 or Guanabenz (**Fig. 6** and **Fig. S4)** included a 15 minutes pre-incubation of the enzymatic components at room temperature (before addition of substrate) with either Sephin1 (Enamine, Cat. No. EN300-195090), Guanabenz (Sigma-Aldrich, Cat. No. D6270), Tautomycin (Calbiochem, Cat. No. 5805551) or an equal volume of DMSO (vehicle).

Reactions were terminated by addition of 10 µL of 3× Laemmli buffer supplemented with 100 mM DTT and heating the samples for 5 minutes at 70°C. A third (10 µL) of the final volume was resolved in 12.5% PhosTag SDS gels

(Wako, Cat. No. NARD AAL-107) at 200 V for 1 hour. Gels were stained with Coomassie Instant Blue and imaged on an Odyssey imager (LI-COR, Lincoln, NE).

ImageJ was used to quantify $eIF2\alpha^P$ dephosphorylation as reflected by the intensity of the fluorescence arising from the Coomassie stain of the $eIF2\alpha^P$ and $eIF2\alpha^0$ bands resolved by the PhosTag SDS-PAGE gels and captured as a TIF file on Odyssey imager. GraphPad Prism v8 was used to fit plot and perform statistical analysis. **Table S3** lists the number of times each experiment was performed.

Conflict of interest: The authors have no conflicts of interest

Author contributions: ACC conceived the study, co-designed and conducted experiments, interpreted the results, created the figures and co-wrote the paper. ZC co-designed the experiments, assisted with the preparation of PP1 from rabbit muscle, interpreted the results, edited the manuscript. MC expressed and purified PP1α from *E. coli*, interpreted the results, edited the manuscript. WP oversaw the expression and purification of PP1α from *E. coli*, interpreted the results, edited the manuscript. MB co-designed the experiments, oversaw the purification of PP1 from rabbit muscle, interpreted the results and edited the manuscript. DR conceived the study, co-designed and conducted experiments, interpreted the results and co-wrote the paper.

References

1.   Pakos-Zebrucka, K., Koryga, I., Mnich, K., Ljujic, M., Samali, A., and Gorman, A. M. (2016) The integrated stress response. *EMBO Rep* **17**, 1374-1395

2.   Dever, T. E., Feng, L., Wek, R. C., Cigan, A. M., Donahue, T. F., and Hinnebusch, A. G. (1992) Phosphorylation of initiation factor 2 alpha by protein kinase GCN2 mediates gene-specific translational control of GCN4 in yeast. *Cell* **68**, 585-596

3.   Harding, H. P., Zhang, Y., Zeng, H., Novoa, I., Lu, P. D., Calfon, M., Sadri, N., Yun, C., Popko, B., Paules, R., Stojdl, D. F., Bell, J. C., Hettmann, T., Leiden, J. M., and Ron, D. (2003) An integrated stress response regulates amino acid metabolism and resistance to oxidative stress. *Mol. Cell* **11**, 619-633

4.   Jousse, C., Oyadomari, S., Novoa, I., Lu, P., Zhang, Y., Harding, H. P., and Ron, D. (2003) Inhibition of a constitutive translation initiation factor 2alpha phosphatase, CReP, promotes survival of stressed cells. *J. Cell Biol.* **163**, 767-775

5.   Novoa, I., Zeng, H., Harding, H., and Ron, D. (2001) Feedback inhibition of the unfolded protein response by GADD34-mediated dephosphorylation of eIF2a. *J. Cell Biol.* **153**, 1011-1022

6.   Brush, M. H., Weiser, D. C., and Shenolikar, S. (2003) Growth arrest and DNA damage-inducible protein GADD34 targets protein phosphatase 1 alpha to the endoplasmic reticulum and promotes dephosphorylation of the alpha subunit of eukaryotic translation initiation factor 2. *Mol. Cell. Biol.* **23**, 1292-1303

7.   Ma, Y., and Hendershot, L. M. (2003) Delineation of a Negative Feedback Regulatory Loop That Controls Protein Translation during Endoplasmic Reticulum Stress. *J. Biol. Chem.* **278**, 34864-34873

8.   Connor, J. H., Weiser, D. C., Li, S., Hallenbeck, J. M., and Shenolikar, S. (2001) Growth arrest and dna damage-inducible protein gadd34 assembles a novel signaling complex containing protein phosphatase 1 and inhibitor 1. *Mol. Cell. Biol.* **21**, 6841-6850.

9.   Choy, M. S., Yusoff, P., Lee, I. C., Newton, J. C., Goh, C. W., Page, R., Shenolikar, S., and Peti, W. (2015) Structural and Functional Analysis of the GADD34:PP1 eIF2alpha Phosphatase. *Cell Rep* **11**, 1885-1891

10.   Chen, R., Rato, C., Yan, Y., Crespillo-Casado, A., Clarke, H. J., Harding, H. P., Marciniak, S. J., Read, R. J., and Ron, D. (2015) G-actin provides substrate-specificity to eukaryotic initiation factor 2alpha holophosphatases. *Elife* **4**, e04871

11.   Malzer, E., Szajewska-Skuta, M., Dalton, L. E., Thomas, S. E., Hu, N., Skaer, H., Lomas, D. A., Crowther, D. C., and Marciniak, S. J. (2013) Coordinate regulation of eIF2alpha phosphorylation by PPP1R15 and GCN2 is required during Drosophila development. *J. Cell Sci.* **126**, 1406-1415

12.   He, B., Gross, M., and Roizman, B. (1998) The gamma134.5 protein of herpes simplex virus 1 has the structural and functional attributes of a protein phosphatase 1 regulatory subunit and is present in a high molecular weight complex with the enzyme in infected cells. *J. Biol. Chem.* **273**, 20737-20743

13.   Crespillo-Casado, A., Chambers, J. E., Fischer, P. M., Marciniak, S. J., and Ron, D. (2017) PPP1R15A-mediated dephosphorylation of eIF2alpha is unaffected by Sephin1 or Guanabenz. *Elife* **6**, e26109

14.   Chambers, J. E., Dalton, L. E., Clarke, H. J., Malzer, E., Dominicus, C. S., Patel, V., Moorhead, G., Ron, D., and Marciniak, S. J. (2015) Actin dynamics tune the integrated

stress response by regulating eukaryotic initiation factor 2alpha dephosphorylation. *Elife* **4**, e04872

15. Harding, H. P., Zhang, Y., Scheuner, D., Chen, J. J., Kaufman, R. J., and Ron, D. (2009) Ppp1r15 gene knockout reveals an essential role for translation initiation factor 2 alpha (eIF2alpha) dephosphorylation in mammalian development. *Proc. Natl. Acad. Sci. U. S. A.* **106**, 1832-1837

16. Marciniak, S. J., Yun, C. Y., Oyadomari, S., Novoa, I., Zhang, Y., Jungreis, R., Nagata, K., Harding, H. P., and Ron, D. (2004) CHOP induces death by promoting protein synthesis and oxidation in the stressed endoplasmic reticulum. *Genes Dev.* **18**, 3066-3077

17. Lin, W., Kunkler, P. E., Harding, H. P., Ron, D., Kraig, R. P., and Popko, B. (2008) Enhanced Integrated Stress Response Promotes Myelinating Oligodendrocyte Survival in Response to Interferon-{gamma}. *Am. J. Pathol.* **173**, 1508-1517

18. D'Antonio, M., Musner, N., Scapin, C., Ungaro, D., Del Carro, U., Ron, D., Feltri, M. L., and Wrabetz, L. (2013) Resetting translational homeostasis restores myelination in Charcot-Marie-Tooth disease type 1B mice. *J. Exp. Med.* **210**, 821-838

19. Wang, L., Popko, B., and Roos, R. P. (2014) An enhanced integrated stress response ameliorates mutant SOD1-induced ALS. *Hum. Mol. Genet.* **23**, 2629-2638

20. Schneider, K., and Bertolotti, A. (2015) Surviving protein quality control catastrophes--from cells to organisms. *J. Cell Sci.* **128**, 3861-3869

21. Carrara, M., Sigurdardottir, A., and Bertolotti, A. (2017) Decoding the selectivity of eIF2alpha holophosphatases and PPP1R15A inhibitors. *Nat. Struct. Mol. Biol.* **24**, 708-716

22. Tsaytler, P., Harding, H. P., Ron, D., and Bertolotti, A. (2011) Selective inhibition of a regulatory subunit of protein phosphatase 1 restores proteostasis. *Science* **332**, 91-94

23. Das, I., Krzyzosiak, A., Schneider, K., Wrabetz, L., D'Antonio, M., Barry, N., Sigurdardottir, A., and Bertolotti, A. (2015) Preventing proteostasis diseases by selective inhibition of a phosphatase regulatory subunit. *Science* **348**, 239-242

24. Peti, W., Nairn, A. C., and Page, R. (2013) Structural basis for protein phosphatase 1 regulation and specificity. *The FEBS journal* **280**, 596-611

25. DeGuzman, A., and Lee, E. Y. (1988) Preparation of low-molecular-weight forms of rabbit muscle protein phosphatase. *Methods Enzymol.* **159**, 356-368

26. Zhou, W., Brush, M. H., Choy, M. S., and Shenolikar, S. (2011) Association with endoplasmic reticulum promotes proteasomal degradation of GADD34 protein. *J. Biol. Chem.* **286**, 21687-21696

27. Mikami, S., Kobayashi, T., Machida, K., Masutani, M., Yokoyama, S., and Imataka, H. (2010) N-terminally truncated GADD34 proteins are convenient translation enhancers in a human cell-derived in vitro protein synthesis system. *Biotechnol. Lett.* **32**, 897-902

28. Kelker, M. S., Page, R., and Peti, W. (2009) Crystal structures of protein phosphatase-1 bound to nodularin-R and tautomycin: a novel scaffold for structure-based drug design of serine/threonine phosphatase inhibitors. *J. Mol. Biol.* **385**, 11-21

29. Hubbard, M. J., and Cohen, P. (1989) Regulation of protein phosphatase-1G from rabbit skeletal muscle. 2. Catalytic subunit translocation is a mechanism for reversible inhibition of activity toward glycogen-bound substrates. *Eur. J. Biochem.* **186**, 711-716

30. Vulsteke, V., Beullens, M., Waelkens, E., Stalmans, W., and Bollen, M. (1997) Properties and phosphorylation sites of baculovirus-expressed nuclear inhibitor of protein phosphatase-1 (NIPP-1). *J. Biol. Chem.* **272**, 32972-32978

31. Verbinnen, I., Ferreira, M., and Bollen, M. (2017) Biogenesis and activity regulation of protein phosphatase 1. *Biochem. Soc. Trans.* **45**, 89-99

32. Brush, M. H., and Shenolikar, S. (2008) Control of cellular GADD34 levels by the 26S proteasome. *Mol. Cell. Biol.* **28**, 6989-7000

33. Perego, J., Mendes, A., Bourbon, C., Camosseto, V., Combes, A., Liu, H., Manh, T. V., Dalet, A., Chasson, L., Spinelli, L., Bardin, N., Chiche, L., Santos, M. A. S., Gatti, E., and Pierre, P. (2018) Guanabenz inhibits TLR9 signaling through a pathway that is independent of eIF2alpha dephosphorylation by the GADD34/PP1c complex. *Sci Signal* **11**

34. Pardee, J. D., and Spudich, J. A. (1982) Purification of muscle actin. *Methods Enzymol.* **85 Pt B**, 164-181

35. Choy, M. S., Hieke, M., Kumar, G. S., Lewis, G. R., Gonzalez-DeWhitt, K. R., Kessler, R. P., Stein, B. J., Hessenberger, M., Nairn, A. C., Peti, W., and Page, R. (2014) Understanding the antagonism of retinoblastoma protein dephosphorylation by PNUTS provides insights into the PP1 regulatory code. *Proc. Natl. Acad. Sci. U. S. A.* **111**, 4097-4102

Table S1. PPP1R15A protein variants used in this study

Name	Sequence	Encoded in plasmid (See Table S2)
PPP1R15A(325-636)-MBP	SGLNDIFEAQKIEWHEGSDPEAECPPCIPPPSAFLKAWVYWPGEDTEEEEDEEEDEDSDSGSDEEEGEAEASSSTPATGVFLKSWVYQPGEDTEEEEDEDSDTGSAEDEREAETSASTPPASAFLKAWVYRPGEDTEEEEDEDVDSEDKEDDSEAALGEAESDPHPSHPDQRAHFRGWGYRPGKETEEEEAAEDWGEAEPCPFRVAIYVPGEKPPPPWAPPRLPLRLQRRLKRPETPTHDPDPETPLKARKVRFSEKVTVHFLAVWAGPAQAARQGPWEQLARDRSRFARRIAQAQEELSPCLTPAARARAWARLRNPPLAPIPALTQTLPSLQAKIEEGKLVIWINGDKGYNGLAEVGKKFEKDTGIKVTVEHPDKLEEKFPQVAATGDGPDIIFWAHDRFGGYAQSGLLAEITPDKAFQDKLYPFTWDAVRYNGKLIAYPIAVEALSLIYNKDLLPNPPKTWEEIPALDKELKAKGKSALMFNLQEPYFTWPLIAADGGYAFKYENGKYDIKDVGVDNAGAKAGLTFLVDLIKNKHMNADTDYSIAEAAFNKGETAMTINGPWAWSNIDTSKVNYGVTVLPTFKGQPSKPFVGVLSAGINAASPNKELAKEFLENYLLTDEGLEAVNKDKPLGAVALKSYEEELAKDPRIAATMENAQKGEIMPNIPQMSAFWYAVRTAVINAASGRQTVDEALKDAQTRITK*	UK1921
PPP1R15A(533-624)MBP	SGLNDIFEAQKIEWHEGSDPGRRLKRPETPTHDPDPETPLKARKVRFSEKVTVHFLAVWAGPAQAARQGPWEQLARDRSRFARRITQAQEELSPCLTPAARARAWARLRNPPLQAKIEEGKLVIWINGDKGYNGLAEVGKKFEKDTGIKVTVEHPDKLEEKFPQVAATGDGPDIIFWAHDRFGGYAQSGLLAEITPDKAFQDKLYPFTWDAVRYNGKLIAYPIAVEALSLIYNKDLPNPPKTWEEIPALDKELKAKGKSALMFNLQEPYFTWPLIAADGGYAFKYENGKYDIKDVGVDNAGAKAGLTFLVDLIKNKHMNADTDYSIAEAAFNKGETAMTINGPWAWSNIDTSKVNYGVTVLPTFKGQPSKPFVGVLSAGINAASPNKELAKEFLENYLLTDEGLEAVNKDKPLGAVALKSYEEELAKDPRIAATMENAQKGEIMPNIPQMSAFWYAVRTAVINAASGRQTVDEALKDAQTRITK*	UK1920
MBP-PPP1R15A(325-512)	MKIEEGKLVIWINGDKGYNGLAEVGKKFEKDTGIKVTVEHPDKLEEKFPQVAATGDGPDIIFWAHDRFGGYAQSGLLAEITPDKAFQDKLYPFTWDAVRYNGKLIAYPIAVEALSLIYNKDLLPNPPKTWEEIPALDKELKAKGKSALMFNLQEPYFTWPLIAADGGYAFKYENGKYDIKDVGVDNAGAKAGLTFLVDLIKNKHMNADTDYSIAEAAFNKGETAMTINGPWAWSNIDTSKVNYGVTVLPTFKGQPSKPFVGVLSAGINAASPNKELAKEFLENYLLTDEGLEAVNKDKPLGAVALKSYEEELVKDPRIAATMENAQKGEIMPNIPQMSAFWYAVRTAVINAASGRQTVDEALKDAQTNSSSNNNNNNNNNLGIEGRISHMSMGGREAECPPCIPPPSAFLKAWVYWPGEDTEEEEDEEEDEDSDSGSDEEEGEAEASSSTPATGVFLKSWVYQPGEDTEEEEDEDSDTGSAEDEREAETSASTPPASAFLKAWVYRPGEDTEEEEDEDVDSEDKEDDSEAALGEAESDPHPSHPDQRAHFRGWGYRPGKETEEEEAAEDWGEAEPCPFRVAIYVDGSEFPAGNHHHHHH*	UK2261
MBP~PPP1R15A(325-636)	MKIEEGKLVIWINGDKGYNGLAEVGKKFEKDTGIKVTVEHPDKLEEKFPQVAATGDGPDIIFWAHDRFGGYAQSGLLAEITPDKAFQDKLYPFTWDAVRYNGKLIAYPIAVEALSLIYNKDLLPNPPKTWEEIPALDKELKAKGKSALMFNLQEPYFTWPLIAADGGYAFKYENGKYDIKDVGVDNAGAKAGLTFLVDLIKNKHMNADTDYSIAEAAFNKGETAMTINGPWAWSNIDTSKVNYGVTVLPTFKGQPSKPFVGVLSAGINAASPNKELAKEFLENYLLTDEGLEAVNKDKPLGAVALKSYEEELVKDPRIAATMENAQKGEIMPNIPQMSAFWYAVRTAVINAASGRQTVDEALKDAQTNSSSNNNNNNNNNLGIEGRISHMSMEAECPPCIPPPSAFLKAWVYWPGEDTEEEEDEEEDEDSDSGSDEEEGEAEASSSTPATGVFLKSWVYQPGEDTEEEEDEDSDTGSAEDEREAETSASTPPASAFLKAWVYRPGEDTEEEEDEDVDSEDKEDDSEAALGEAESDPHPSHPDQRAHFRGWGYRPGKETEEEEAAEDWGEAEPCPFRVAIYVPGEKPPPPWAPPRLPLRLQRRLKRPETPTHDPDPETPLKARKVRFSEKVTVHFLAVWAGPAQAARQGPWEQLARDRSRFARRITQAQEELSPCLTPAARARAWARLRNPPLAPIPALTQTLPSHHHHHHSG*	UK2258
MBP-PPP1R15A(325-636)	MKIEEGKLVIWINGDKGYNGLAEVGKKFEKDTGIKVTVEHPDKLEEKFPQVAATGDGPDIIFWAHDRFGGYAQSGLLAEITPDKAFQDKLYPFTWDAVRYNGKLIAYPIAVEALSLIYNKDLLPNPPKTWEEIPALDKELKAKGKSALMFNLQEPYFTWPLIAADGGYAFKYENGKYDIKDVGVDNAGAKAGLTFLVDLIKNKHMNADTDYSIAEAAFNKGETAMTINGPWAWSNIDTSKVNYGVTVLPTFKGQPSKPFVGVLSAGINAASPNKELAKEFLENYLLTDEGLEAVNKDKPLGAVALKSYEEELVKDPRIAATMENAQKGEIMPNIPQMSAFWYAVRTAVINAASGRQTVDEALKDAQTNSSSNNNNNNNNNLGIEGRISHMSMGGREAECPPCIPPPSAFLKAWVYWPGEDTEEEEDEEEDEDSDSGSDEEEGEAEASSSTPATGVFLKSWVYQPGEDTEEEEDEDSDTGSAEDEREAETSASTPPASAFLKAWVYRPGEDTEEEEDEDVDSEDKEDDSEAALGEAESDPHPSHPDQRAHFRGWGYRPGKETEEEEAAEDWGEAEPCPFRVAIYVPGEKPPPPWAPPRLPLRLQRRLKRPETPTHDPDPETPLKARKVRFSEKVTVHFLAVWAGPAQAARQGPWEQLARDRSRFARRIAQAQEELSPCLTPAARARAWARLRNPPLAPIPALTQTLPSVDGSEFPAGNHHHHHH*	UK2260

Table S2. Plasmids used in this study

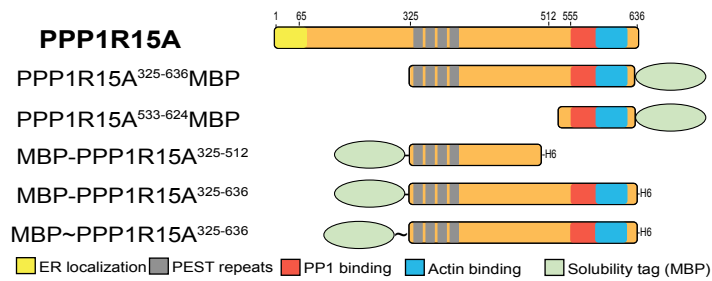| Lab number	Lab name	Description	Abbreviation	Reference
UK105	eIF2a-NM_pET30a	His6-tagged human eIF2a 1-185 pET-30a(+)"	eIF2a	PMID 15341733
UK168	PerkKD-pGEX4T-1	Bacterial expression plasmid for mouse PERK kinase domain	PERK	PMID 9930704
UK622	PGV_PP1G_1-323_V1	Bacterial expression plasmid for full-length PP1 phosphatase catalytic domain	PP1G	PMID 25774600
UK1920*	huPPP1R15A_533_624_malE_pGEX_TEV_AviTag (MP1)	Bacterial expression plasmid for N-tern AviTagged human GADD34 533-624	R15A533-624-MBP	PMID: 28447936
UK1921*	huPPP1R15A_325_636_malE_pGEX_TEV_AviTag (MP4	Bacterial expression plasmid for N-tern AviTagged human GADD34 325-624	R15A325-636-MBP	PMID: 28447936
UK2258*	huPPP1R15A_325-636_pMAL-c5X-H6 (AB)**	Bacterial expression plasmid for MBP_1R15A(325-636)-H6	MBP~R15A325-636	PMID: 28759048
UK2260*	MBP_huPPP1R15A_325-636_H6_pMAL-c5X-His	Bacterial expression plasmid for MBP_R15A(325-636)-H6	MBP-R15A325-636	This study
UK2261*	MBP_huPPP1R15A_325-512_H6_pMAL-c5X-His	Bacterial expression plasmid for MBP_R15A(325-512)-H6 (N-term)	MBP-R15A325-512	This study
UK2264	PP1A_7-330_RP1B (MPC)	Bacterial expression plasmid for H6-TEV-rabbit PP1A 7-330 Peti lab (Addgene Plasmid# 26566)	PP1a	PMID: 18992256

*The sequence of the proteins encoded by these plasmids is available as Table S1

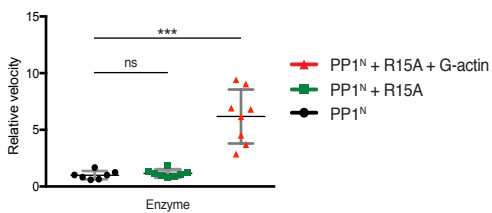**A gift from Anne Bertolotti's laboratory

Table S3. Number of repeats for the different experiments

Figures		Repeats
1	a	n/a
	b	2
	c	2
2	a	3
	b	3
	c	3
3	a	3
	b	3
4	a	2
	b	2
5	a	3
	b	2
6	a	3
	b	2
7	a	n/a
S1	a	1
	b	1
S2	a	3
	b	1
S3	a	n/a
	b	1
S4	a	2
	b	1
	c	2
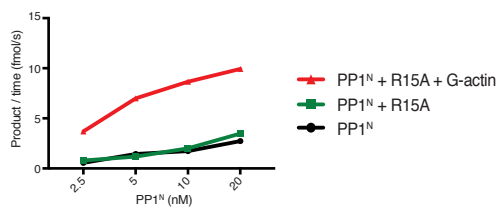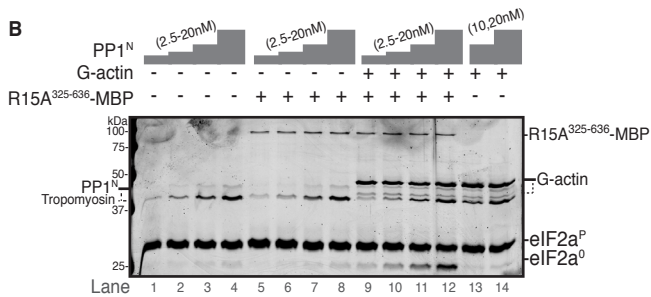
Figure 1. G-actin stimulates PPP1R15A-dependent eIF2α^P dephosphorylation by either PP1^N or PP1α

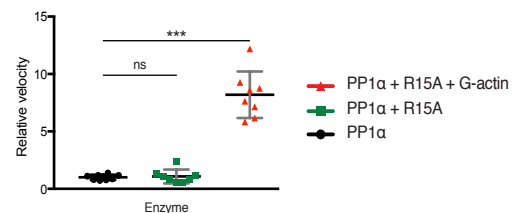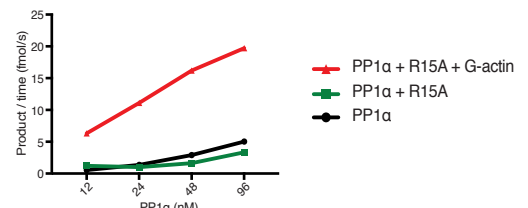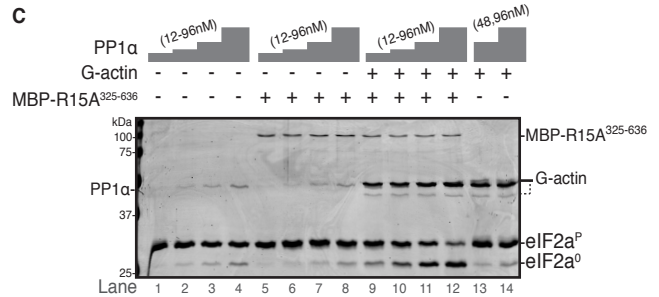*A*, Cartoon representation of human PPP1R15A protein (1-674) and the different constructs used in this study (sequence provided in Table S1). Key residues used for truncated versions of the proteins in this study are annotated. The ER localization domain and the proline, glutamate, serine and threonine-rich (PEST) repeats are highlighted as are the PP1 and G-actin binding sites in the conserved C-terminal region. MBP solubility tag is also represen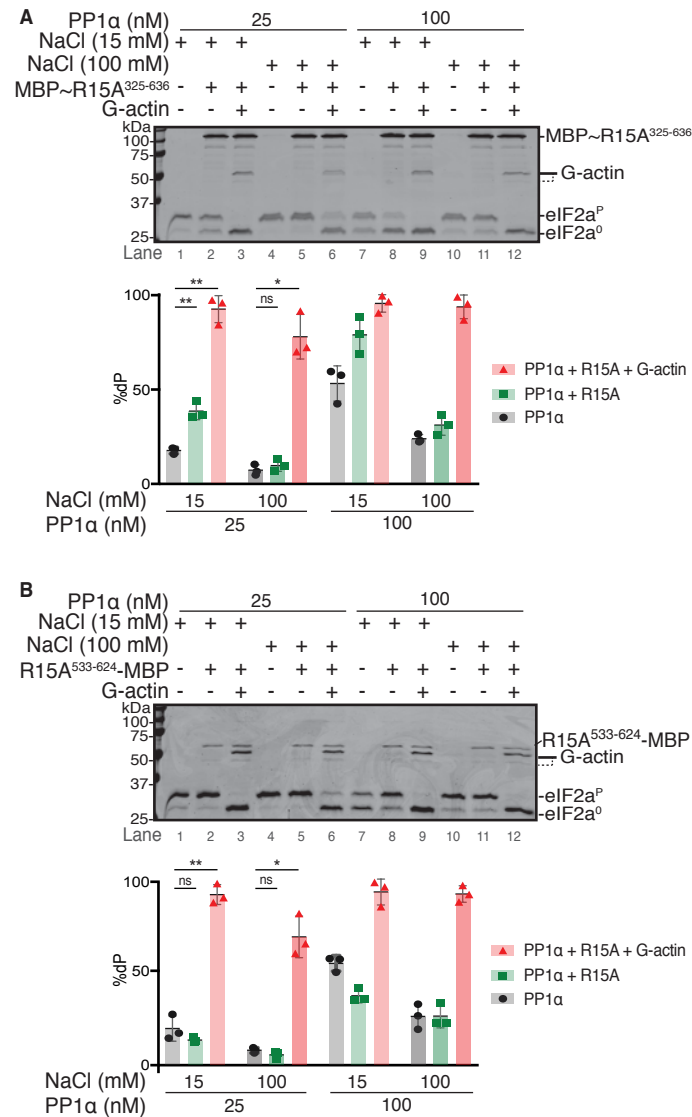ted in the cartoons of the constructs. *B*, <u>Upper panel</u>: Coomassie-stained PhosTag-SDS-PAGE containing resolved samples of dephosphorylation reactions (30 minutes at 30°C) in which 2 μM eIF2α^P was dephosphorylated by PP1^N purified from rabbit skeletal muscle in the presence or absence of PPP1R15A$^{325-636}$-MBP (50 nM) and/or G-actin (400 nM).The position of the various protein species is indicated. eIF2α^P and eIF2α^0 refer to the phosphorylated and non-phosphorylated form of the bacterially-expressed N-terminal domain (residues 1-185) of eIF2α, respectively. Note that both G-actin and PP1^N preparation gave rise to two bands: a major full-length species and minor degradation product, in the case of G-actin, and a PP1and tropomyosin band in the case of PP1^N (see also Fig. *S1*). Shown is a representative experiment of two independent repetitions performed. <u>Middle panel</u>: Plot of the rate of eIF2α^P dephosphorylation as a function of the concentration of PP1^N from lanes 1 to 12 of experiment above. <u>Bottom panel</u>: Plot of the velocity of each enzyme relative to the mean of velocity of PP1 alone calculated from all the informative reactions in the two repeats of this experiment. Statistical significance derived from Mann-Whitney test (ns, n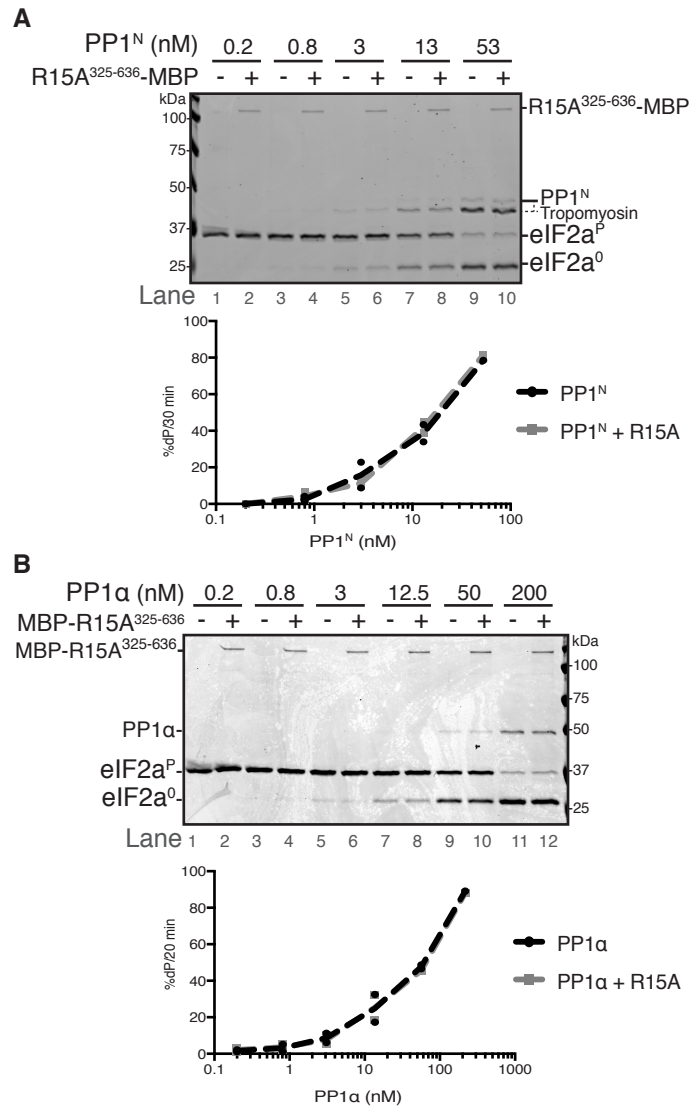on significant, $p > 0.05$; ***, $p \leq 0.001$). *C*, as in "*B*" but using bacterially-expressed PP1α as the catalytic subunit (96, 48, 24 or 12 nM), MBP-PPP1R15A$^{325-636}$ (50 nM) and G-actin (400 nM). The assays were performed during 20 minutes at 30°C. Shown is a representative experiment of two independent repetitions performed.
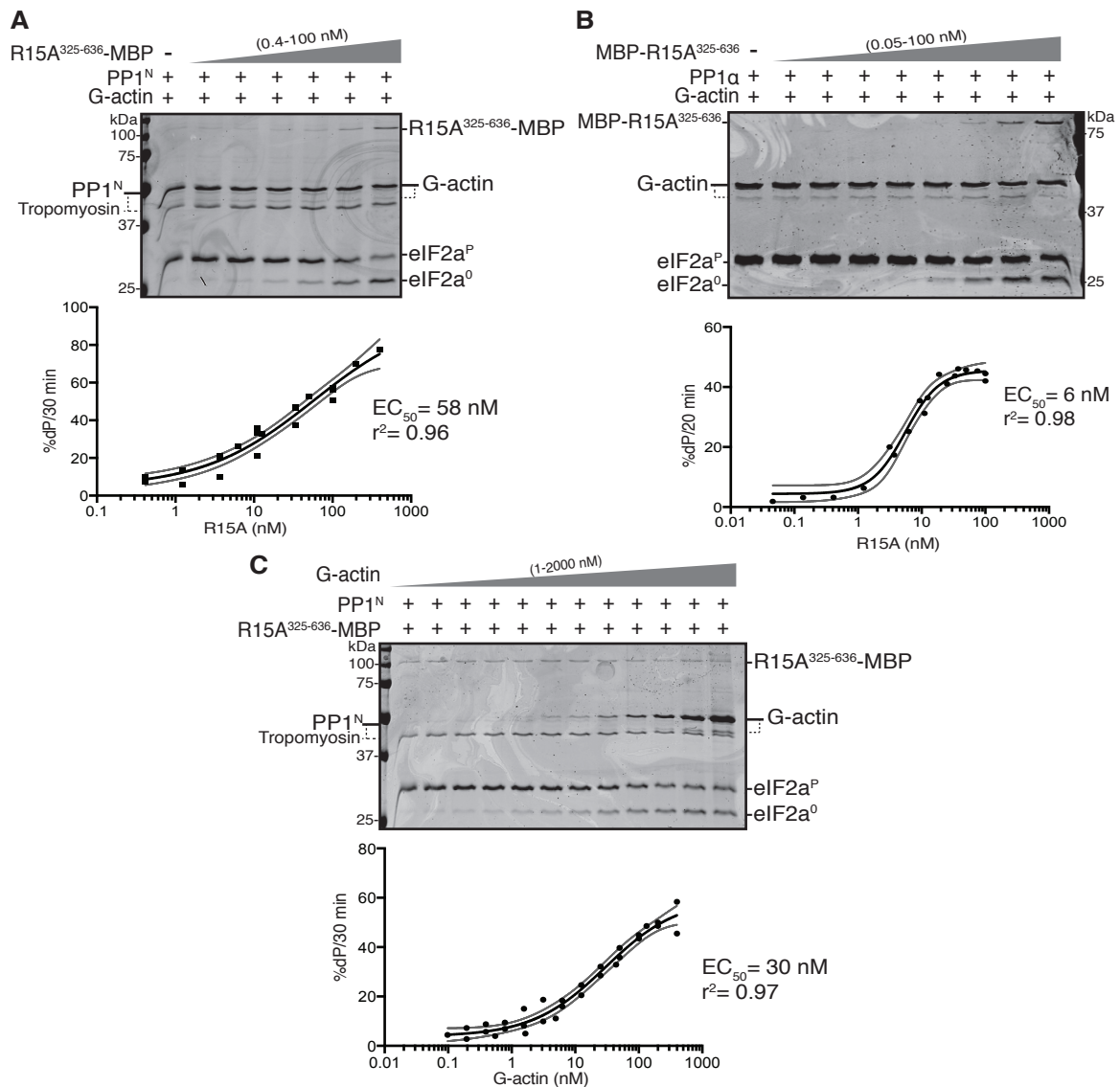
Figure 2. The source of catalytic subunit does not affect the kinetics of PPP1R15A and G-actin-mediated stimulation of eIF2α^P dephosphorylation. *A*, <u>Upper panel</u>: Coomassie-stained PhosTag-SDS-PAGE of dephosphorylation reactions (30 minutes at 30˚C), in which 2 μM eIF2α^P was dephosphorylated by PP1^N (20 nM) in presence of G-actin (400 nM) and increasing concentrations of PPP1R15A$^{325-636}$-MBP (0-100 nM). Shown is a representative experiment of three independent experiments performed. <u>Lower panel</u>: Plot of the rate of dephosphorylation of eIF2α^P as a function of PPP1R15A$^{325-636}$-MBP concentration, from the three experiments performed. The EC$_{50}$ was calculated using the "[Agonist] vs. response - variable slope (four parameters)" function in GraphPad Prism v7. The grey lines represent the 95% confidence interval of the fitting. Shown are values obtained for EC$_{50}$ and information of goodness of the fit (r^2). *B*, as in "*A*" but using bacterially-expressed PP1α (24 nM) and increasing concentrations of MBP-PPP1R15A$^{325-636}$ (0-100 nM) in reactions performed over 20 minutes at 30˚C. Shown is a representative experiment of three independent experiments performed. *C*. As in "*A*" but with fixed concentrations of PP1^N (20 nM) and PPP1R15A$^{325-636}$-MBP (50 nM) and varying the concentrations of G-actin (1-2000 nM). Shown is a representative experiment of three independent experiments performed.

Figure 3. PPP1R15A$^{325\text{-}636}$ accelerates eIF2α^P dephosphorylation by PP1α in a low ionic strength buffer.

 A, <u>Upper panel</u>: Coomassie-stained PhosTag-SDS-PAGE containing resolved samples of dephosphorylation reactions (30 minutes at 30˚C) in which 2 μM eIF2α^P was dephosphorylated by PP1α (25 or 100 nM) in the presence or absence of MBP~PPP1R15A$^{325\text{-}636}$ (1 μM) with or without G-actin (400 nM) in low (15 mM NaCl) or physiological (100 mM NaCl) ionic strength buffer. Shown is a representative experiment of three independent repetitions performed. <u>Lower panel</u>: Plot of the percentage of eIF2α^P dephosphorylation at the different conditions from the experiment above and the two other repeats performed. Statistical significance derived from paired two tailed t-test, (ns, non significant, $p > 0.05$; *, $p \leq 0.05$; **, $p \leq 0.01$). *B*, as in "*A*" but using PPP1R15A$^{533\text{-}624}$-MBP (200 nM). Shown is a representative experiment of three independent repetitions performed.

Figure 4. At physiological ionic strength and in the absence of G-actin, PPP1R15A is unable to stimulate dephosphorylation of eIF2αP (despite an extended incubation of 16h). *A*, <u>Upper panel</u>: Coomassie-stained PhosTag-SDS-PAGE containing dephosphorylation reactions (16 hours at 30˚C) in which 2 μM eIF2α^P was dephosphorylated by the indicated concentration of PP1^N in the presence or absence of PPP1R15A$^{325-636}$-MBP (50 nM). Quantification of percentage of dephosphorylation (%dP) is shown below the image. Shown is a representative experiment of two independent repetitions performed.<u>Lower panel</u>: Plot of the rate of dephosphorylation of eIF2α^P as a function of PP1^N concentration. Data was obtained by quantification of bands of image shown above and the other repeat performed. *B*, as in "*A*" but using PP1α as the source of catalytic subunit and MBP-PPP1R15A$^{325-636}$ (50 nM) as the regulatory subunit. Shown is a representative experiment of two independent repetitions performed**.**

Figure 5. The C-terminal portion of PPP1R15A is sufficient to promote eIF2αP dephosphorylation. *A,* <u>Upper panel</u>: Coomassie-stained PhosTag-SDS-PAGE containing resolved samples from dephosphorylation reactions (30 minutes at 30˚C) in which 2 μM eIF2α^P was dephosphorylated by PP1^N (20 nM) in the presence of G-actin (400 nM) and increasing concentrations of PPP1R15A$^{533-624}$-MBP (0-100 nM). Shown is a representative experiment of three independent repetitions performed. <u>Lower panel</u>: Plot of the rate of dephosphorylation of eIF2α^P as a function of PPP1R15A$^{533-624}$-MBP concentration, from the three experiments performed. The EC$_{50}$ was calculated using the "[Agonist] vs. response - variable slope (four parameters)" function in GraphPad Prism v7. The grey lines represent the 95% confidence interval of the fitting. Shown are values obtained for EC$_{50}$ and information of goodness of the fit (r^2). *B.* as in "*A*" but using PP1α (24 nM) in presence of MBP-PPP1R15A$^{325-636}$ (24 nM), G-actin (400 nM) and increasing concentrations of MBP-PPP1R15A$^{325-512}$ as a competitor (0-8 μM). The assays were performed during 20 minutes at 30˚C. Lane 8, loaded with only MBP-PPP1R15A$^{325-512}$ shows the absence of a species co-migrating with eIF2α^0 (which might otherwise obscure an inhibitory effect on dephosphorylation). Lanes 9 and 10 control for the dependence of enzymatic activity on PPP1R15A and G-actin in this experiment. Quantification of percentage of dephosphorylation (%dP) is shown below the image. Shown is a representative experiment of two independent repetitions performed.

A

PP1α	+	-	-	+	-	+	+	+	+	+
MBP-R15A$^{325\text{-}636}$	-	+	-	-	+	+	+	+	+	+
G-actin	-	-	+	+	+	-	-	+	+	+
Sephin1 (100 μM)								+		
Tau (80 nM)									+	+

%dP	16	0	0	12	0	12	12	49	50	0
Lane	1	2	3	4	5	6	7	8	9	10

B

PP1α	+	-	-	+	-	+	+	+	+	+
MBP-R15A$^{325\text{-}636}$	-	+	-	-	+	+	+	+	+	+
G-actin	-	-	+	+	+	-	-	+	+	+
GBZ (100 μM)								+		
Tau (80 nM)									+	+

%dP	23	0	0	17	0	15	11	55	53	0
Lane	1	2	3	4	5	6	7	8	9	10
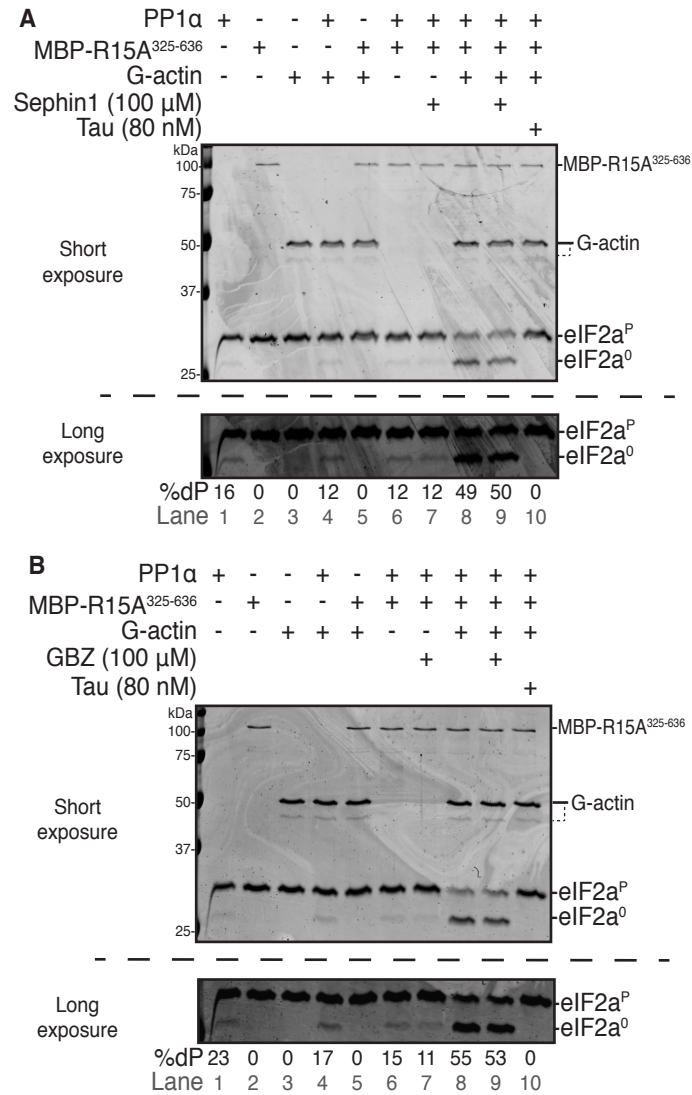
Figure 6. Neither Sephin1 nor GBZ interfere with eIF2α^P dephosphorylation *A*, Coomassie-stained PhosTag-SDS-PAGE containing resolved samples from dephosphorylation reactions (20 minutes, 30˚C) in which 2 μM eIF2α^P was dephosphorylated by PP1α (24 nM) in presence or absence of MBP-PPP1R15A$^{325\text{-}636}$ (60 nM) and/or G-actin (400 nM). The components were pre-incubated as specified with either Sephin1 (100 μM), Tautomycin (80 nM) or DMSO (vehicle) for 15 minutes at room temperature before being added to the reaction. The bottom panel shows a long exposure of the relevant section of the image above corresponding to the phosphorylated and non-phosphorylated forms of eIF2α. Quantification of percentage of dephosphorylation (%dP) is shown below the image. Shown is a representative experiment of three independent experiments performed. *B*, as in "*A*" but with Guanabenz (GBZ). Shown is a representative experiment of two independent experiments performed.
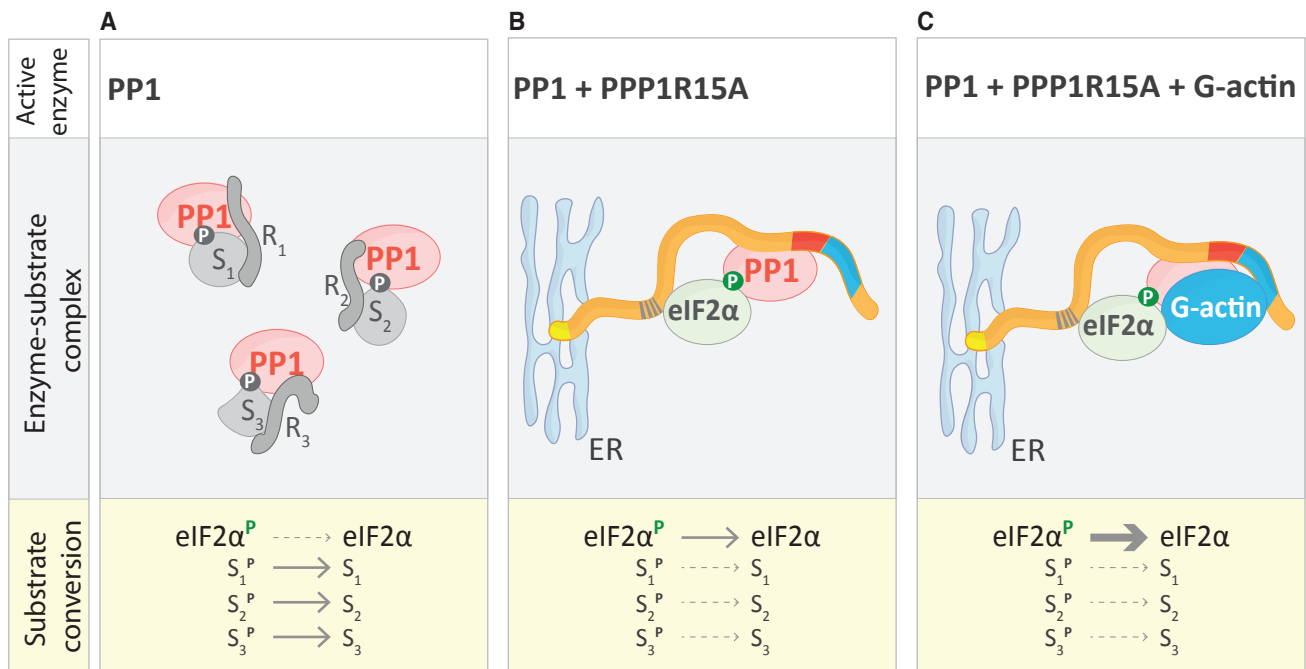
Figure 7. Model depicting PPP1R15A's role in regulating eIF2αP dephosphorylation. *A*, In absence of PPP1R15A the cellular pool of catalytic subunit (PP1) is preferentially bound by a variety of regulatory subunits (R_1, R_2, R_3) which direct its phosphatase activity towards their specific substrates (S_1, S_2, S_3), excluding eIF2α^P. In the substrate conversion section, see the preferential dephosphorylation of substrates S_1, S_2 and S_3 (solid arrow) compared to eIF2α (dotted arrow). *B*, Rising levels of PPP1R15A recruit PP1 away from other regulatory subunits, redirecting its phosphatase activity towards eIF2α^P by excluding other substrates. In the substrate conversion section, observe the inverted preferential dephosphorylation of substrates compared to "*A*". *C*, When present, G-actin joins the PPP1R15A-PP1 holophosphatase, increasing its intrinsic eIF2α^P-directed catalytic activity. In the substrate conversion section, see the increased arrow thickness for eIF2αP dephosphorylation compared to "*B*".
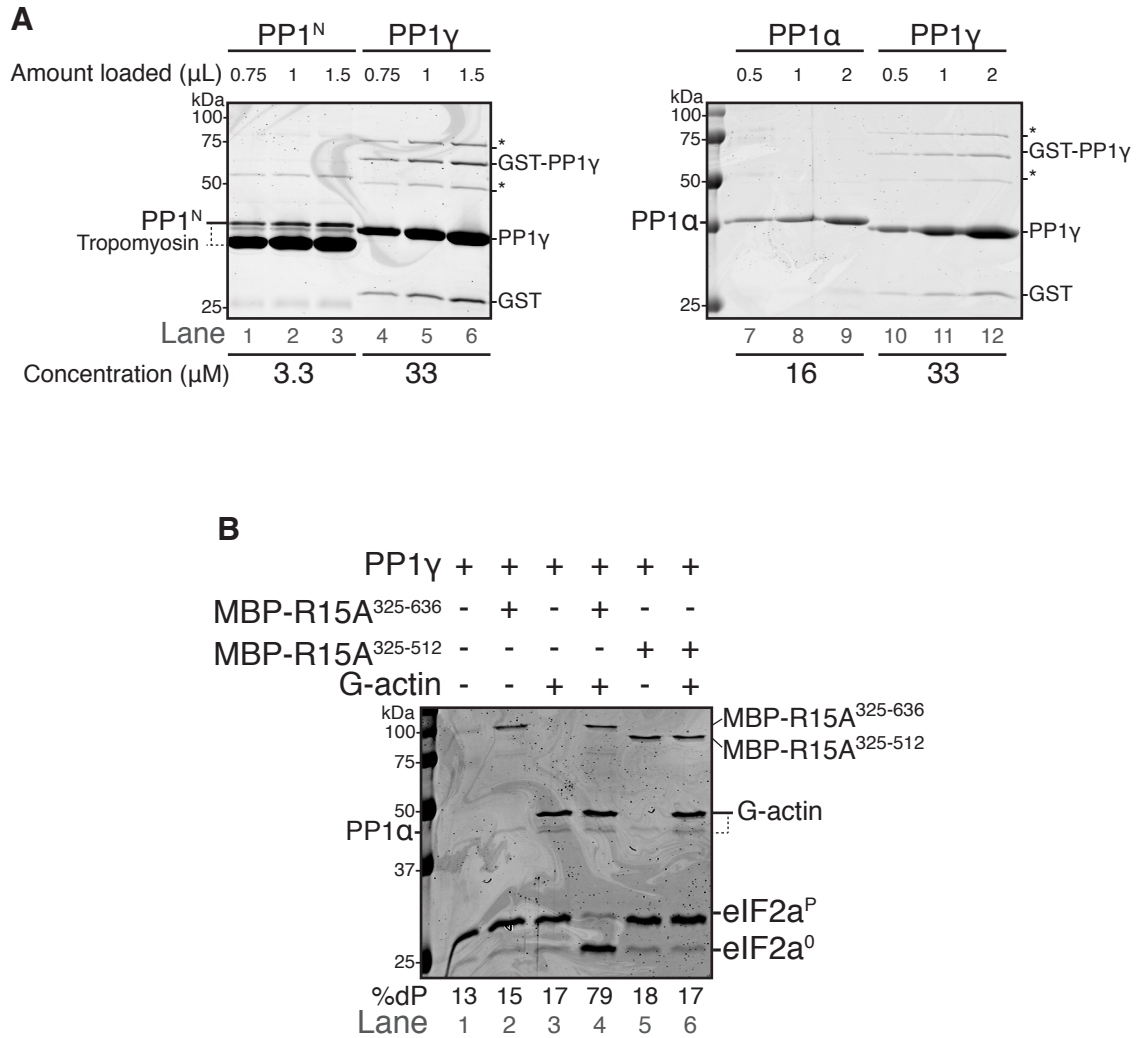
Supporting Figure 1. Analysis of the purity of the different sources of PP1. *A*, Coomassie-stained SDS-PAGE in which different amounts of PP1 sample have been resolved. The PP1^N preparation gave rise to two bands: a PP1 and tropomyosin band. The PP1γ preparation contained some free Glutathione S Transferase (GST) and GST-PP1 fusion protein from the purification steps, as well as other minor contaminants (*). The PP1 concentration in the different preparations is shown below the panels, calculated using PP1γ as a reference. *B*, Coomassie-stained PhosTag-SDS-PAGE containing resolved samples from dephosphorylation reactions (as in Fig. 1*A* and *B*) in which 2 μM eIF2α^P was dephosphorylated using bacterially-expressed PP1γ (24 nM) in presence or absence of MBP-PPP1R15A$^{325-636}$ (50 nM), MBP-PPP1R15A$^{325-512}$ (50 nM) and/or G-actin (400 nM) for 20 minutes at 30°C. Quantification of percentage of dephosphorylation (%dP) is shown below the image.
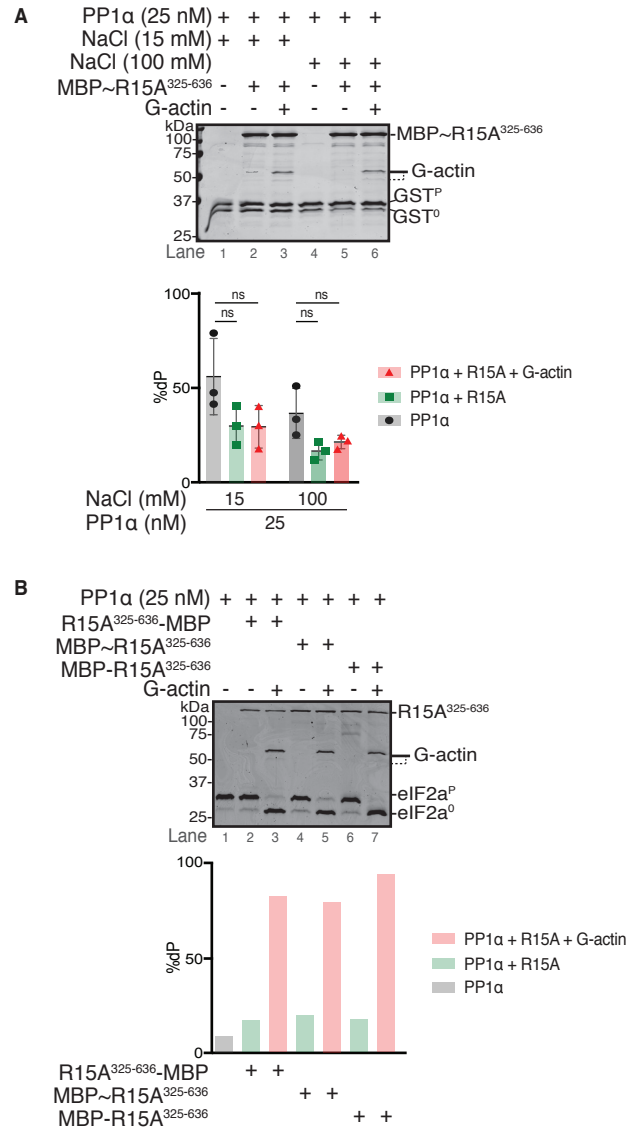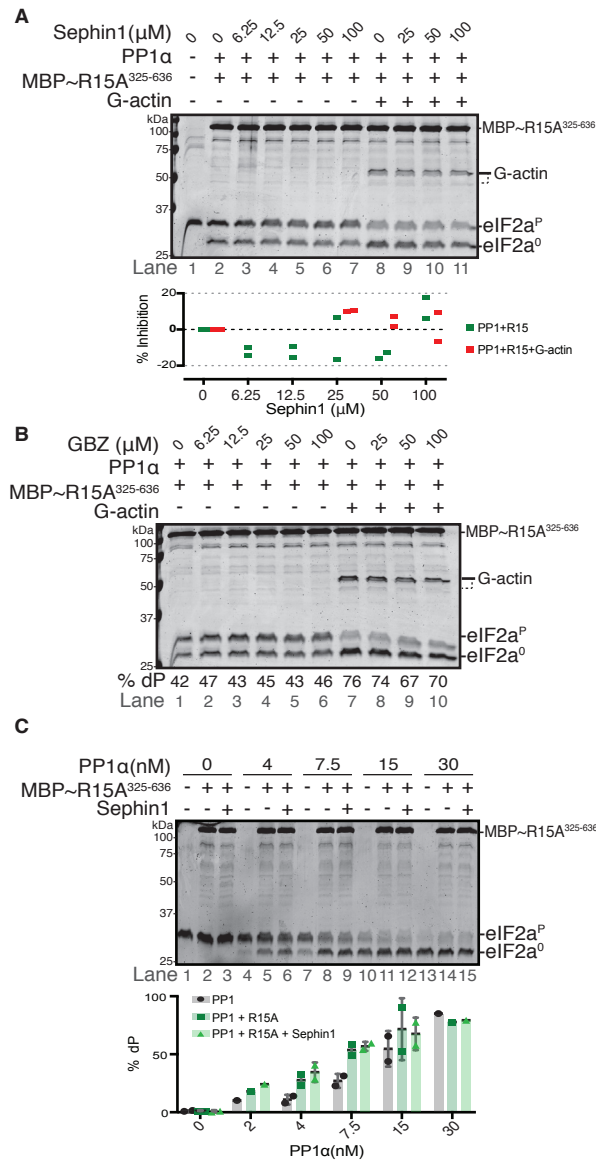
Supporting Figure 2. PPP1R15A$^{325\text{-}636}$ selectively accelerates eIF2α^P dephosphorylation by PP1α in a low ionic strength buffer. *A*, <u>Upper panel</u>: Coomassie-stained PhosTag-SDS-PAGE containing resolved samples of dephosphorylation reactions (30 minutes at 30˚C) in which 2 μM GST^P (a non specific substrate) was dephosphorylated by PP1α (25nM) in the presence or absence of MBP~PPP1R15A$^{325\text{-}636}$ (1 μM) with or without G-actin (400 nM) in low (15 mM NaCl) ionic strength buffer. Shown is a representative experiment of three independent repetitions performed. <u>Lower panel</u>: Plot of the percentage of eIF2α^P dephosphorylation at the different conditions from the experiment above and the two other repeats performed. Statistical significance derived from paired two tailed t-test,(ns, non significant, p > 0.05). *B*, as in "*A*" but using PPP1R15A$^{325\text{-}636}$-MBP (200 nM), MBP~PPP1R15A$^{325\text{-}636}$ (200 nM) or MBP-PPP1R15A$^{325\text{-}636}$ (200 nM) as regulatory subunits with and without G-actin (400 nM) in low (15 mM NaCl) ionic strength buffer.
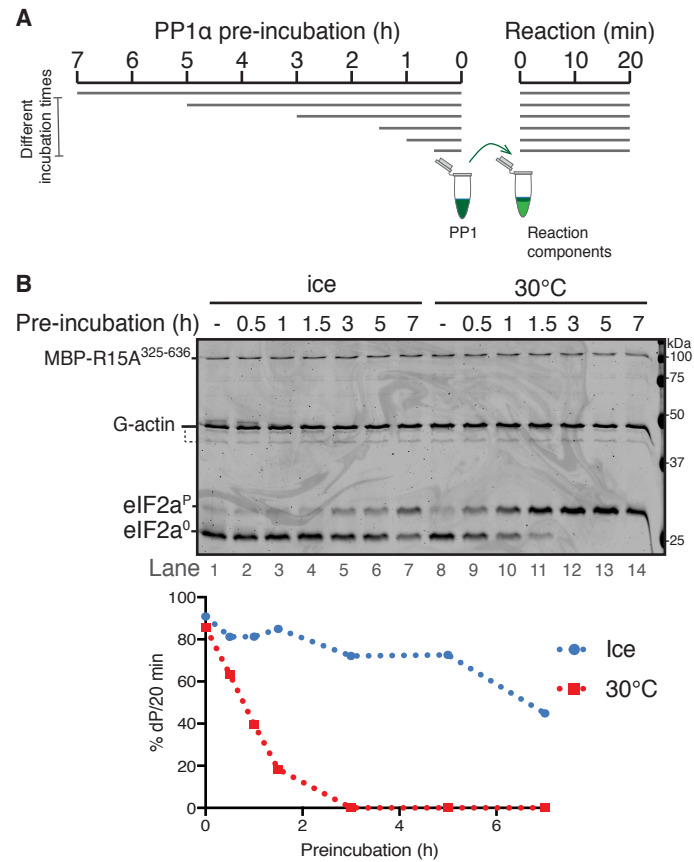
Supporting Figure 3. PP1α is an unstable enzyme. *A*, Schema of the experiment. Samples of PP1α (at 240 nM) were pre-incubated for the indicated period of time, either on ice or at 30˚C, before being diluted into a eIF2α^P dephosphorylation reaction. *B*, Upper panel: Coomassie-stained PhosTag-SDS-PAGE containing samples from dephosphorylation reactions (20 minutes at 30˚C) in which 2 μM eIF2α^P was dephosphorylated by the pre-incubated PP1α (60 nM) in presence of MBP-PPP1R15A$^{325-636}$ (60 nM) and G-actin (400 nM). Lower panel. Plot of the rate of dephosphorylation of eIF2α^P as a function of pre-incubation time of PP1α catalytic subunit. Data was obtained by quantification of bands of image shown above.

Supporting Figure 4. Neither Sephin1 nor GBZ interfere with eIF2α^P dephosphorylation. *A*, Upper panel: Coomassie-stained PhosTag-SDS-PAGE containing resolved samples from dephosphorylation reactions (30 minutes, 30˚C) in which 2 μM eIF2α^P were dephosphorylated by PP1α (25 nM) in presence of MBP~PPP1R15A$^{325-636}$ (1 μM) in either low ionic strength buffer (15 mM NaCl, without G-actin, lanes 2-7), or in physiological ionic strength buffer (100 mM, with 400 nM G-actin, lanes 8-11) in presence of Sephin1 (or DMSO carrier). Shown is a representative of two independent experiments performed. Lower panel: Plot of percentage inhibition observed in all samples of the experiment shown above and its repeat (calculated separately in each experiment relative to the no-compound condition, 0 μM). *B*, as in "A" but with Guanabenz (GBZ). Percentage of dephosphorylation shown below the image. *C*, Upper panel: as in "*A*" but following extended incubation time of dephosphorylation reactions (18 hour, 30˚C) performed in presence of the indicated concentrations of PP1α in the absence or presence of MBP~PPP1R15A$^{325-636}$ (1 μM) and Sephin1 (100 μM). Shown is a representative of two independent experiments performed. Lower panel: Plot of the percentage of eIF2α^P dephosphorylation from the experiment above and the other repeat performed